NASA TR R-392

NASA TECHNICAL REPORT

NASA TR R-392

EFFECTS OF CIRCULAR GEOMETRY IN SIMULATION OF CONVECTION IN ROTATING-SPACECRAFT TANKS

by E. Dale Martin, Barrett S. Baldwin, and Margaret Covert

Ames Research Center
Moffett Field, Calif. 94035

NATIONAL AERONAUTICS AND SPACE ADMINISTRATION • WASHINGTON, D. C. • OCTOBER 19

1. Report No. NASA TR R–392	2. Government Accession No.	3. Recipient's Catalog No.
4. Title and Subtitle EFFECTS OF CIRCULAR GEOMETRY IN SIMULATION OF CONVECTION IN ROTATING-SPACECRAFT TANKS		5. Report Date October 1972 6. Performing Organization Code
7. Author(s) E. Dale Martin, Barrett S. Baldwin, and Margaret Covert		8. Performing Organization Report No. A–4513
9. Performing Organization Name and Address NASA-Ames Research Center Moffett Field, Calif., 94035		10. Work Unit No. 136–13–05–09–00–21 11. Contract or Grant No.
12. Sponsoring Agency Name and Address National Aeronautics and Space Administration Washington, D. C., 20546		13. Type of Report and Period Covered Technical Report 14. Sponsoring Agency Code
15. Supplementary Notes		

16. Abstract

For computational simulation of the convection and mixing of stratified fluid in a rotating tank (such as used in Apollo flights) with time-dependent rotation, the Navier-Stokes convection problem is formulated for a circular-tank configuration. The final equations result from a general approximate theory derived previously for combined forced and contained natural convection in a time-dependent rotating system. The equations are cast in terms of vorticity and stream function in a form most convenient for computation, with a convenient transformed coordinate system, and appropriate boundary conditions are derived for use in subsequent numerical computations. Accurate representations for the cryogenic supercritical oxygen thermodynamic properties are used in the computations, and a highly efficient numerical finite-difference scheme and computational method, used previously by Lomax and Bailey, are employed.

Computations in both square and circular two-dimensional tank configurations simulate the motion and heating of the oxygen in spherical tanks under conditions corresponding to Apollo flights. The circular-tank calculations are performed to compare with previous square-tank results and to confirm the previous general conclusions. The effects of rotation reversal maneuvers, spin-up maneuvers, and heater cycles on the evolution of temperature distributions and on the pressure and potential for pressure collapse are examined and compared for the two configurations.

The results show that appreciable mixing can be achieved in a short time by small rotation maneuvers to prevent pressure collapse. The conclusions from previous calculations of a square-tank configuration are confirmed.

17. Key Words (Suggested by Author(s))	18. Distribution Statement
Convection Stratified fluid Rotating system Compressible Viscous Apollo spacecraft	Unclassified – Unlimited

19. Security Classif. (of this report)	20. Security Classif. (of this page)	21. No. of Pages	22. Price*
Unclassified	Unclassified	22	$3.00

*For sale by the National Technical Information Service, Springfield, Virginia 22151

CONTENTS

EFFECTS OF CIRCULAR GEOMETRY IN SIMULATION OF CONVECTION IN ROTATING-SPACECRAFT TANKS

E. Dale Martin, Barrett S. Baldwin, and Margaret Covert

Ames Research Center

SUMMARY

For computational simulation of the convection and mixing of stratified fluid in a rotating tank (such as used in Apollo flights) with time-dependent rotation, the Navier-Stokes convection problem is formulated for a circular-tank configuration. The final equations result from a general approximate theory derived previously for combined forced and contained natural convection in a time-dependent rotating system. The equations are cast in terms of vorticity and stream function in a form most convenient for computation, with a convenient transformed coordinate system, and appropriate boundary conditions are derived for use in subsequent numerical computations. Accurate representations for the cryogenic supercritical oxygen thermodynamic properties are used in the computations, and a highly efficient numerical finite-difference scheme and computational method, used previously by Lomax and Bailey, are employed.

Computations in both square and circular two-dimensional tank configurations simulate the motion and heating of the oxygen in spherical tanks under conditions corresponding to Apollo flights. The circular-tank calculations are performed to compare with previous square-tank results and to confirm the previous general conclusions. The effects of rotation reversal maneuvers, spin-up maneuvers, and heater cycles on the evolution of temperature distributions and on the pressure and potential for pressure collapse are examined and compared for the two configurations.

The results show that appreciable mixing can be achieved in a short time by small rotation maneuvers to prevent pressure collapse. The conclusions from previous calculations of a square-tank configuration are confirmed.

INTRODUCTION

This report describes extensions of a previous study (ref. 1) of combined forced and natural convection and mixing of a thermally stratified fluid in a spacecraft tank with time-dependent rotation.

The background of the study is described in some detail in reference 2, but for completeness here a description of the physical problem is provided below. The study applies to spacecraft fluid-storage systems in general (including, e.g., those in orbiting space stations); but the study arose

in connection with the oxygen tanks in the Apollo spacecraft, so the particular conditions imposed and the specific results obtained refer to Apollo oxygen tanks.

In spacecraft, oxygen and hydrogen are stored in a supercritical cryogenic state because a large mass of fluid can be stored at high density (small volume) and at pressures low enough for reasonably lightweight tanks and high enough to ensure adequate supply to various systems. In Apollo, the oxygen tanks are spheres with inside diameters of 63.5 cm (25 in.) and distances from their centers to the spacecraft axis of 91.44 cm (3 ft) and 152.4 cm (5 ft). (The 3-ft rotation arm is used in the computations to be described later.) Initially, the tanks are loaded with 150 kg (330 lb) of liquid oxygen. Then the oxygen is heated by an internal electric heater to vaporize the oxygen. The heater is then operated periodically to maintain a system design pressure of $620 \times 10^4 \pm 24 \times 10^4$ N/m^2 ($\sim$900 $\pm$ 35 psia). When the pressure drops to the lower design limit because of withdrawal of fluid, the heater is automatically turned on. When the pressure rises to the upper limit, the heater is switched off. These heater cycles and pressure cycles are discussed in later sections of the report.

Under these conditions, the oxygen temperature can be of order 150° K, near the critical point. The fluid is supercritical and is not distinguishable as either a liquid or a gas. At these conditions, a small change in temperature can cause a substantial pressure drop. If the fluid is significantly stratified in density and temperature and is suddenly mixed, such a resulting pressure drop (also called pressure collapse or pressure decay) may even drive the fluid into the undesirable two-phase state and may render inoperative the systems supplied by the oxygen-storage system. For understanding of these concepts, the reader should refer to Kamat and Abraham (ref. 3).

During portions of flights by spacecraft such as Apollo, the conditions can develop for which pressure collapse can occur. When the craft is in a zero-gravity condition with no accelerations, each heater cycle results in increasingly severe temperature gradients near the heater. The gradients decay very slowly because of the inefficiency of pure heat condition for energy transfer. Therefore, to prevent the potentially dangerous levels of stratification, frequent mixing must be provided. Prior to the Apollo 13 accident, the fluid inside the tanks was circulated by means of electric fans. The Apollo 13 Review Board found that the electric fans played a part in the accident that aborted that mission, and the oxygen tanks for subsequent missions were redesigned to eliminate the fans. An analysis determined that the stratification problem could be crucial, so other means of stirring, or inducing convection, were needed. One problem was to determine the adequacy of vehicle rotation and maneuvers to produce sufficient convection and mixing through the body forces due to temperature differences and rotational accelerations.

As a means for estimating the mixing effectiveness of rotation and rotational maneuvers, the fluid convection can be simulated by numerical computations. For this purpose a set of equations was developed (ref. 4) that represent a general approximate theory for the Navier-Stokes description of fluid convection in a rotating system, including the influence of both the effective buoyancy body forces due to temperature and density stratifications and the arbitrary time-dependent rotation of the tank. The equations reduce to a generalization of the Boussinesq approximation in the special case of steady rotation with variable buoyancy body forces, but also properly represent the forced convection due to time-dependent rotation. The equations are valid for combined forced and contained natural convection, whereas previous treatments of convection in rotating systems had dealt with either pure natural convection or pure forced convection (e.g., see ref. 5, sec. F, 22; and refs. 6 and 7).

For convenience in the use of the numerical methods employed (and in keeping with the spirit of Lighthill's description of the flow development and its relation to vorticity ref. 8, pp. 57–60), the equations were cast in terms of the vorticity and stream functions in reference 4. For the first numerical calculations (refs. 9 and 10), convection in a rotating square two-dimensional tank was treated. Although three-dimensional effects such as axial flow due to Ekman-layer suction (e.g., ref. 6) and development of Taylor vortices (see ref. 7) could not be represented in a two-dimensional formulation, the first numerical treatment by this theory (refs. 9 and 10) yielded significant information regarding the adequacy of vehicle rotation and of rotation reversal for mixing.

The first numerical treatment of the Apollo oxygen tank convection employed the square-tank configuration for convenience in developing the numerical methods, since many of the essential two-dimensional effects could be simulated. A two-dimensional *circular* tank, with a small circular interior boundary at the center and a heat source near the center, may more closely simulate the actual spherical oxygen tank containing the central circular-cylindrical capacitance gage and the heater, as described in reference 2. Therefore, one purpose of this report is to extend the previous study to circular geometry – i.e., to formulate, in a form particularly suited to subsequent numerical computation, the problem of convection in a circular tank and to compare the results of computations for the circular geometry with those for the square geometry. The flow equations that are used result from the general approximate theory (based on a small-density-variation approximation) developed in reference 4 for combined forced and contained natural convection, with influence by both buoyancy body forces and time-dependent rotation of the vehicle. The final equations for computation are put into forms very similar to those used for the square tank in reference 4. The accurate representations of thermodynamic properties from reference 11 are used, as well as the special procedures from reference 12 for analysis of the thermodynamic states resulting from the small-density-variation approximation.

FLOW EQUATIONS AND PROBLEM DEFINITION FOR CONVECTION IN A ROTATING CIRCULAR TANK

Configuration and Flow Equations

The circular-tank configuration for analysis of the convection is shown in sketch (a). The r, θ polar-coordinate system is fixed relative to the tank, with θ measured from a line perpendicular to the rotation arm (from the tank center to the center of rotation, of length R_C). The radius vector from the rotation center O to a point r, θ in the tank is denoted by $\underset{\sim}{R}$, with components R_r and R_θ in the directions of the unit vectors $\underset{\sim}{e}_r$ and $\underset{\sim}{e}_\theta$ (the directions of increasing r and θ, respectively):

$$\underset{\sim}{R} = \underset{\sim}{e}_r R_r + \underset{\sim}{e}_\theta R_\theta \tag{1a}$$

where

$$R_r = r + R_C \sin\theta \tag{1b}$$

$$R_\theta = R_C \cos\theta \tag{1c}$$

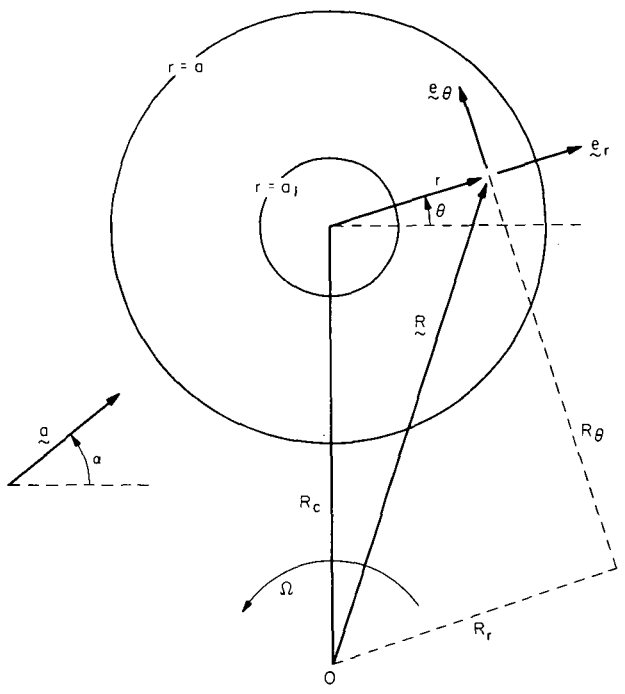

Sketch (a). Circular tank configuration.

The time-dependent angular velocity Ω is positive when counterclockwise. Then in the r,θ coordinates the effective body force per unit mass, given by equation (2.12) in reference 4 is

$$\underset{\sim}{g} = \underset{\sim}{e}_r g_r + \underset{\sim}{e}_\theta g_\theta \tag{2a}$$

where

$$g_r = R_r \Omega^2 + 2\Omega v_\theta + \dot{\Omega} R_\theta - a_r \tag{2b}$$

$$g_\theta = R_\theta \Omega^2 - 2\Omega v_r - \dot{\Omega} R_r - a_\theta \tag{2c}$$

in which a_r and a_θ are the components of a prescribed vector $\underset{\sim}{a}$, which is an arbitrary time-dependent linear acceleration of point O in the noninertial system of coordinates fixed on the tank, relative to an inertial system. (As an effective body force per unit mass, $\underset{\sim}{a}$ may be taken to include any body forces acting on the fluid in the inertial reference frame.) As shown in sketch (a), $\underset{\sim}{a}$ may be prescribed by its magnitude $|\underset{\sim}{a}|$ and instantaneous relative direction α, so that

$$\underset{\sim}{a} = \underset{\sim}{e}_r a_r + \underset{\sim}{e}_\theta a_\theta \tag{3a}$$

with

$$a_r = |\underset{\sim}{a}|\cos(\alpha - \theta) \tag{3b}$$

$$a_\theta = |\underset{\sim}{a}|\sin(\alpha - \theta) \tag{3c}$$

Also in equations (2), $\dot{\Omega}$ is defined to be $d\Omega/dt$, and v_r and v_θ are the respective r and θ components of the fluid velocity vector $\underset{\sim}{V}$ measured relative to the coordinate system fixed on the rotating tank:

$$\underset{\sim}{V} = \underset{\sim}{e}_r v_r + \underset{\sim}{e}_\theta v_\theta \tag{4}$$

The approximate system of flow equations developed in reference 4 is based on the full compressible Navier-Stokes equations with the assumption that the thermodynamic state variables, density ρ, pressure p, and temperature T, have small variations in space and relatively slow variations in time. The approximation proceeds by a small-perturbation approach referenced to the

thermodynamic state (ρ_O, p_O, T_O) representing nearly constant values of ρ, p, and T that are averages over the space of the tank at a given time. For the small-perturbation analysis, one writes

$$\rho = \rho_O(1 + \delta) \tag{5a}$$

where

$$\delta \approx -\beta(T - T_O) \qquad |\delta| << 1 \tag{5b}$$

$$\beta \equiv \left[-\frac{1}{\rho} \left(\frac{\partial \rho}{\partial T} \right)_p \right]_o \tag{5c}$$

Along with the above assumptions, the specific enthalpy is taken to be independent of pressure; and the transport properties – viscosity $\mu = \rho_O \nu$ and thermal conductivity k – are assumed to be nearly constant in space and slowly varying in time. That is, spatial gradients of μ and k are neglected, but μ, k, and the specific heat c_p are all allowed to vary with time and to depend on the spatial distribution of temperature and on the average pressure at any time.

To satisfy the approximate equation of conservation of mass resulting from assuming $|\delta| << 1$ ($\nabla \cdot \underset{\sim}{V} = 0$), one can define a stream function (eqs. (2.33e) in ref. 4) such that

$$v_r = \frac{1}{r} \frac{\partial \psi}{\partial \theta}, \quad v_\theta = -\frac{\partial \psi}{\partial r} \tag{6}$$

It is advantangeous to use as a primary variable the vorticity (Lighthill, reference 8, pp. 57-60), which is defined by

$$\underset{\sim}{\omega} \equiv \nabla \times \underset{\sim}{V} \tag{7a}$$

where for two-dimensional flow (with the unit vector $\underset{\sim}{e}_z = \underset{\sim}{e}_r \times \underset{\sim}{e}_\theta$):

$$\underset{\sim}{\omega} = \underset{\sim}{e}_z \omega \tag{7b}$$

and the scalar ω is (cf. ref. 4, eqs. (2.63) and (2.64)):

$$\omega = \frac{1}{r} \frac{\partial}{\partial r} (r v_\theta) - \frac{1}{r} \frac{\partial v_r}{\partial \theta}$$

$$= -\nabla^2 \psi = -\frac{1}{r^2} \left[r \frac{\partial}{\partial r} \left(r \frac{\partial \psi}{\partial r} \right) + \frac{\partial^2 \psi}{\partial \theta^2} \right] \tag{8}$$

From reference 4, eq. (2.58c), the approximate equation for the rate of change of vorticity, derived from conservation of momentum, is

$$\frac{\partial \omega}{\partial t} + \frac{1}{r}\left[\frac{\partial}{\partial r}(rv_r\omega) + \frac{\partial}{\partial \theta}(v_\theta \omega)\right] = \frac{\nu}{r^2}\left[r\frac{\partial}{\partial r}\left(r\frac{\partial \omega}{\partial r}\right) + \frac{\partial^2 \omega}{\partial \theta^2}\right]$$

$$-g_\theta \beta \frac{\partial T}{\partial r} + g_r \beta \left(\frac{1}{r}\frac{\partial T}{\partial \theta}\right) - 2\dot{\Omega} \qquad (9)$$

The approximate energy equation, with Dp/Dt neglected (ref. 4, eq. (2.84) with (2.85) and (2.75)), is

$$\frac{\partial T}{\partial t} + \frac{1}{r}\left[\frac{\partial}{\partial r}(rv_r T) + \frac{\partial}{\partial \theta}(v_\theta T)\right] = \left(\frac{k}{\rho_o c_p}\right)\frac{1}{r^2}\left[r\frac{\partial}{\partial r}\left(r\frac{\partial T}{\partial r}\right) + \frac{\partial^2 T}{\partial \theta^2}\right] + \frac{\nu}{c_p}\Phi \qquad (10a)$$

where the dissipation function Φ is

$$\Phi = 2\left[\left(\frac{\partial v_r}{\partial r}\right)^2 + \left(\frac{1}{r}\frac{\partial v_\theta}{\partial \theta} + \frac{v_r}{r}\right)^2\right] + \left[r\frac{\partial}{\partial r}\left(\frac{v_\theta}{r}\right) + \frac{1}{r}\frac{\partial v_r}{\partial \theta}\right]^2 \qquad (10b)$$

Application of Boundary Conditions

Initially (at $t = 0$) a temperature distribution is specified according to a prescribed temperature stratification; and $v_r = v_\theta = 0$ everywhere (assumed-rigid-body rotation) so that

$$\omega = 0 \quad \text{everywhere initially.} \qquad (11)$$

Boundary conditions for $t \geqslant 0$ must be specified on ψ, ω, and T for application to equations (8), (9), and (10).

On the boundaries $r = a$ (outer tank wall) and $r = a_1$ (interior circular boundary representing the capacitance gage in the Apollo oxygen tank), the conditions of no normal mass flux and no slip are

$$\left.\begin{matrix} r = a \\ r = a_1 \end{matrix}\right\} : \quad v_r = v_\theta = 0 \qquad (12a)$$

or

$$\left(\frac{\partial \psi}{\partial \theta}\right)_b = \left(\frac{\partial \psi}{\partial r}\right)_b = 0 \qquad (12b)$$

where the subscript b indicates a value at a boundary. The application of these conditions to the Poisson equation (8) for ψ and the parabolic equation (9) for ω must be formulated in a manner to be compatible with the numerical-solution technique. Such application is described as follows.

For an arbitrary smooth two-dimensional boundary with coordinates s and n measuring respectively distances along and perpendicular to the boundary, and with curvature $K = K(s)$ of the boundary surface, the conditions are

$$\textit{no mass flux:}\quad v_n = \frac{-1}{1+Kn}\frac{\partial \psi}{\partial s} = 0 \quad \text{on the boundary} \tag{13a}$$

$$\textit{no slip:}\qquad v_s = \frac{\partial \psi}{\partial n} = 0 \quad \text{on the boundary} \tag{13b}$$

where v_s and v_n are the respective velocity components tangent and normal to the boundary. Again with the subscript b denoting a boundary value, equation (13a) can be replaced by

$$\textit{no mass flux:}\quad \psi_b = c(t) \tag{14}$$

and equation (13b) is

$$\textit{no slip:}\quad \left(\frac{\partial \psi}{\partial n}\right)_b = 0 \tag{15}$$

Also in terms of the coordinates s and n, it can be shown that conditions (13) along with $\nabla^2 \psi = -\omega$ give

$$\left(\frac{\partial^2 \psi}{\partial n^2}\right)_b = -\omega_b \tag{16a}$$

At a small distance ϵ measured perpendicular to a smooth boundary, Taylor's series for $\psi = \psi_\epsilon$ is

$$\psi_\epsilon = \psi_b + \epsilon \left(\frac{\partial \psi}{\partial n}\right)_b + \frac{1}{2}\epsilon^2 \left(\frac{\partial^2 \psi}{\partial n^2}\right)_b + \ldots$$

so that insertion of equations (15) and (16a) gives the approximate condition

$$\omega_b \approx \frac{-2(\psi_\epsilon - \psi_b)}{\epsilon^2}. \tag{16b}$$

Equations (14) and either (15) or (16) can be used to represent (13).

In most problems, ψ_b can be specified. In that case, the conventional approach is to specify $\psi_b = 0$ (eq. (14)) for application to equation (8) for the ψ field. Effectively, condition (13a) has then been applied, and ψ is known everywhere at the current time step of the computation. Then condition (16b) is specified as a boundary condition at the current time step in solving the vorticity equation by an explicit scheme for interior values of ω at the next time step. Effectively the no-slip condition, (13b) or (15), has then been applied through (16b) to the vorticity equation.

It may happen, as is the case in the present problem at the interior boundary, that ψ_b is not known. One could apply (14) to equation (8) and iterate on the value of $c(t)$ at each time step, but this would consume machine-computing time. Therefore, a suggested alternative is to apply the no-slip condition (15) to the Poisson equation (8) for ψ; then when ψ is known at the current time step, effectively use the no-mass-flux condition incorporated into the Taylor series that results in condition (16b) (with ψ_b constant at a given time) for application to solving the vorticity equation (9). (This alternative approach is believed to be new.)

From the above discussion, for the circular-tank problem one can now specify the following boundary conditions on ψ and ω for application to equations (8) and (9), respectively,

$$r = a: \quad \psi = 0 \tag{17a}$$

$$\omega = \omega_a = \frac{-2(\psi)_{a-\Delta r}}{(\Delta r)^2} \tag{17b}$$

$$r = a_1: \quad \frac{\partial \psi}{\partial r} = 0 \tag{18a}$$

$$\omega = \omega_{a_1} = \frac{-2(\psi_{a_1 + \Delta r} - \psi_{a_1})}{(\Delta r)^2} \tag{18b}$$

The application of (17) and (18) is illustrated in sketch (b).

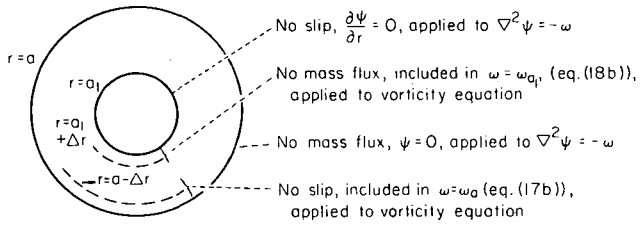

Sketch (b). Application of boundary conditions.

For application to equation (10a), the heat flux or $\partial T/\partial r$ can be specified on all boundaries (with value zero for insulated boundaries). A heat source at some interior point near $r = a_1$ can be specified to represent the power input from the heater.

In θ, all variables must be periodic with period 2π. One variation in the numerical application of the boundary condition on vorticity is discussed on page 13 of the section on Computational Procedure and in the Discussion section, page 18. The above conditions could be applied without alteration if a sufficiently fine computation mesh were used.

The function $\Omega(t)$ must be prescribed and, in the example of sudden rotation reversal, can be represented by

$$\Omega(t) = \Omega_o[-1 + 2S(t)] \tag{19a}$$

$$\dot{\Omega}(t) = 2\Omega_o\dot{S}(t) \tag{19b}$$

where Ω_o is a constant angular velocity, $S(t)$ is the unit step function,

$$S(t) = 0 \quad t < 0 \tag{20a}$$

$$= 1 \quad t \geqslant 0 \tag{20b}$$

and $\dot{S}(t)$ is the Dirac delta function. Simple numerical approximations to equations (20) may be used, such as a linear change of $S(t)$ from 0 to 1 between $t = 0$ and small time t_1, for which the corresponding approximation to $\dot{S}(t)$ is the constant value $1/t_1$ for $0 \leqslant t < t_1$ and zero outside that time interval (used also in ref. 4).

Transformation of Variable and Dimensionless Equations for Computation

To facilitate numerical computations using a "Poisson solver" for the computation step involving solution of equation (8) for ψ, it is convenient to make the transformation

$$\zeta = \ln \frac{r}{a} \tag{21}$$

which puts the Laplacian operator into a form similar to the rectangular-coordinate form.

Then with L as an arbitrary length, and ΔT as an arbitrary constant reference temperature difference, the following dimensionless variables and parameters are introduced:

$$\left.\begin{aligned}
&\xi = \xi(\zeta) = \frac{r}{L} = \left(\frac{a}{L}\right)e^{\zeta}\ , \quad \tau = \frac{\nu t}{L^2} \\
&\omega^* = \frac{\omega L^2}{\nu}\ , \quad H = \frac{T - T_O}{\Delta T}\ , \quad \Psi = \frac{\psi}{\nu} \\
&U = \frac{v_r L}{\nu}\ , \quad V = \frac{v_\theta L}{\nu} \\
&\Omega^*(\tau) = \frac{2\Omega(t)}{\nu L^{-2}}\ , \quad \Omega_O^* = \frac{2\Omega_O}{\nu L^{-2}} \\
&G_1 = Gr\,\frac{g_r}{\Omega_O{}^2 L}\ , \quad G_2 = Gr\,\frac{g_\theta}{\Omega_O{}^2 L} \\
&a_1{}^* = \frac{a_r}{\Omega_O{}^2 L}\ , \quad a_2{}^* = \frac{a_\theta}{\Omega_O{}^2 L} \\
&\Phi^* = \frac{L^4}{\nu^2}\ \Phi
\end{aligned}\right\} \qquad (22a)$$

with:

$$\left.\begin{aligned}
&\text{Reynolds number} = Re = \frac{\Omega_O L^2}{\nu} \\
&\text{Prandtl number} = Pr = \frac{\rho_O \nu c_p}{k} \\
&\text{Grashof number} = Gr = \frac{(\Omega_O{}^2 L)\, L^3 \beta \Delta T}{\nu^2} \\
&\text{Eckert number} = Ec = \frac{(\Omega_O L)^2}{c_p \Delta T}
\end{aligned}\right\} \qquad (22b)$$

(This particular nondimensionalization is not motivated by any order of magnitude considerations for the present problem but was used for convenience in comparing test calculations with results obtained from similar previous calculations.) Equations (6), (8), (9), and (10) become, in *dimensionless* form (dropping the stars from ω^*, Ω^*, Φ^*, $a_1{}^*$, and $a_2{}^*$ from here on):

$$\frac{\partial \omega}{\partial \tau} + \frac{1}{\xi^2}\left[\frac{\partial}{\partial \zeta}\ (\xi U \omega) + \frac{\partial}{\partial \theta}\ (\xi V \omega)\right] = \frac{1}{\xi^2}\left(\frac{\partial^2 \omega}{\partial \zeta^2} + \frac{\partial^2 \omega}{\partial \theta^2}\right) + \frac{1}{\xi}\left(-G_2\,\frac{\partial H}{\partial \zeta} + G_1\,\frac{\partial H}{\partial \theta}\right) - \frac{d\Omega}{d\tau} \qquad (23)$$

$$\frac{\partial H}{\partial \tau} + \frac{1}{\xi^2}\left[\frac{\partial}{\partial \zeta}(\xi UH) + \frac{\partial}{\partial \theta}(\xi VH)\right] = \frac{1}{Pr}\left(\frac{1}{\xi^2}\right)\left(\frac{\partial^2 H}{\partial \zeta^2} + \frac{\partial^2 H}{\partial \theta^2}\right) + \frac{Ec}{Re^2}\Phi \tag{24}$$

$$\frac{\partial^2 \Psi}{\partial \zeta^2} + \frac{\partial^2 \Psi}{\partial \theta^2} = -\xi^2 \omega \tag{25}$$

$$U = \frac{1}{\xi}\frac{\partial \Psi}{\partial \theta}, \quad V = \frac{-1}{\xi}\frac{\partial \Psi}{\partial \zeta} \tag{26}$$

where

$$G_1 = \frac{Gr}{Re^2}\left[(\xi + \sin\theta)\frac{1}{4}\Omega^2 + \Omega V + (\cos\theta)\frac{1}{2}\frac{d\Omega}{d\tau}\right] - Gr\, a_1 \tag{27a}$$

$$G_2 = \frac{Gr}{Re^2}\left[(\cos\theta)\frac{1}{4}\Omega^2 - \Omega U - (\xi + \sin\theta)\frac{1}{2}\frac{d\Omega}{d\tau}\right] - Gr\, a_2 \tag{27b}$$

$$\Phi = \frac{2}{\xi^2}\left[\left(\frac{\partial U}{\partial \zeta}\right)^2 + \left(\frac{\partial V}{\partial \theta} + U\right)^2\right] + \frac{1}{\xi^2}\left(\frac{\partial V}{\partial \zeta} - V + \frac{\partial U}{\partial \theta}\right)^2 \tag{28}$$

and where ξ is the function of ζ defined in equations (22a). (In eq. (24), the time derivative of T_O in H has been neglected.)

The initial conditions for the dimensionless variables in equations (23)through (26) are

$$\left.\begin{aligned} \tau = 0: \quad & U = V = \omega = 0 \\ & H(\zeta, \theta, 0) \text{ prescribed} \end{aligned}\right\} \tag{29}$$

The transformation of variables can be thought of, and the equations analyzed, in terms of a rectangular ζ, θ mesh as illustrated in sketch (c), corresponding to the r,θ polar coordinates shown.

The boundary conditions in the ζ,θ plane include the periodic condition for all dependent variables: at each ζ in sketch (c), all dependent variables must have the same values at $\theta = 2\pi$ as at $\theta = 0$.

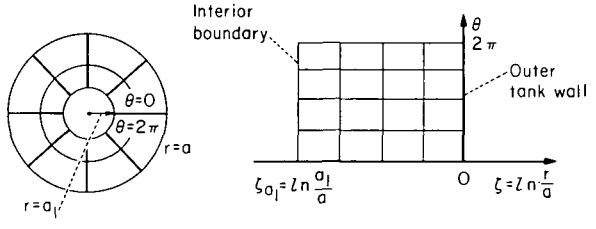

Sketch (c). Transformation of coordinates.

The boundary conditions at the outer tank wall corresponding to conditions (17) are

$$\zeta = 0 \; : \quad \Psi = 0 \tag{30a}$$

$$\omega = \frac{-2(\Psi)_{\zeta = 0} - |\Delta\zeta|}{(a/L)^2 \; (\Delta\zeta)^2} \tag{30b}$$

At the interior circular boundary, conditions (18) become

$$\zeta = \zeta_{a_1} \equiv \ln \frac{a_1}{a} \; : \quad \frac{\partial \Psi}{\partial \zeta} = 0 \tag{31a}$$

$$\omega = \frac{-2 \left[(\Psi)_{\zeta = \zeta_{a_1}} + |\Delta\zeta| - (\Psi)_{\zeta = \zeta_{a_1}} \right]}{(a_1/L)^2 \; (\Delta\zeta)^2} \tag{31b}$$

for application to equations (25) and (23) respectively. For specified heat flux $-k(\partial T/\partial r)$ at $r = a$ and $r = a_1$, the corresponding values of

$$\left(\frac{\partial H}{\partial \zeta} \right)_{\zeta = 0} = \frac{a}{k(\Delta T)} \left(k \frac{\partial T}{\partial r} \right)_{r = a} \tag{32a}$$

$$\left(\frac{\partial H}{\partial \zeta} \right)_{\zeta = \zeta_{a_1}} = \frac{a_1}{k(\Delta T)} \left(k \frac{\partial T}{\partial r} \right)_{r = a_1} \tag{32b}$$

are specified for application to equation (24).

The dimensionless function $\Omega(\tau)$ and $d\Omega/d\tau$ may be specified, for example, as in the discussion of equations (19) and (20), with t and t_1 replaced by τ and τ_1.

COMPUTATIONAL PROCEDURE

The numerical method for the integration of equations (23) through (25) is very similar to that described in reference 9, which should be referred to for details. An explicit finite difference procedure is used for equations (23) and (24) that employs the predictor-corrector method of reference 13. The main difference in the overall procedure is that the stream-function equation in reference 9 was solved at each step in the integration over time by a Buneman recursive-cyclic-reduction technique, whereas equation (25) with the periodic boundary condition at $\theta = 0$ and $\theta = 2\pi$ and with conditions (30a) and (31a) is solved in the same context in the present method by a Fast-Fourier-Transform technique as described by Hockney in reference 14. The thermodynamic relations and attendant computational procedures are described in references 11 and 12. Boundary conditions on the dimensionless relative temperature H are imposed corresponding to a specified

heat leak through the walls. A time-dependent value of H is imposed on computational grid points selected to represent the heater used to overcome pressure decreases due to removal of fluid from the tank.

Although pressure gradients must be considered in the momentum equations, pressure gradients are negligible in the energy equation for the low-velocity cryogenic oxygen flows under consideration. In the energy equation the variation of pressure with time has only a cumulative effect that does not affect the motion of the fluid. As discussed in reference 4 the only important coupling between the energy and momentum equations is through temperature gradients and convection of temperature variations. As a result, for the purpose of finding the motion of the fluid, the density can be considered a function of temperature with pressure as a slowly varying time-dependent parameter that is uniform in the tank. Time-dependent temperature and density distributions then result from integration of the equations of motion over short time steps. Computation of the evolution of pressure and other thermodynamic quantities is described in reference 12. One such quantity of particular interest is the potential pressure decay, which is the drop in pressure that would result from complete adiabatic mixing of the stratified fluid. Thus, the potential pressure decay is a measure of the pressure loss that could result from spacecraft maneuvering after a given level of stratification has built up from nonuniform heating of the fluid in a near zero-g environment (see, e.g., ref. 3).

Several expedient remedies for removal of difficulties arising from application of the numerical method are discussed in references 10 and 12. A uniform spacing of computational grid points was employed. It was found that it is not possible to resolve adequately the viscous boundary layer that develops near the wall. One could use the boundary conditions (17b) and (18b) precisely if a sufficiently fine mesh were used. However, to avoid excessive computing time a coarse mesh (17 X 17 computation points) was employed in most of the calculations. It then was found necessary to put limits on the absolute value of vorticity so that extreme (unreal) viscous stresses would not be propagated to the interior from the walls when large flow velocities occurred near the walls. Thus, the boundary conditions (17b) and (18b) were overridden and replaced by constant values when the computed values exceeded the fixed upper limit. Most of the calculations used an upper limit equal to four times the vorticity corresponding to the solid body fluid motion associated with a spacecraft rotation reversal with a total change of 1.6667×10^{-3} revolution per sec (6 revolutions per hour). Sample calculations were made with an upper limit half as large to establish that variations of thermodynamic quantities, such as pressure and potential pressure decay, were insensitive to this approximation. The effect of the approximation on the results is considered further in the discussion section of this report.

RESULTS

Rotation Reversal Maneuver

Calculations were made for both square and circular tanks in which the spacecraft was taken to be rotating initially at 8.333×10^{-4} revolutions per sec (3 revolutions per hour). An assumed initial stratified state was imposed in each case with temperature varying linearly across the tank. The warmer fluid was placed in the stable position toward the center of rotation. As shown in reference 10, this linear type of temperature distribution does occur after prolonged heater cycling during rotation at a steady rate. In the absence of spacecraft maneuvering other than constant rotation, the calculations showed a very slow decrease in potential pressure decay as expected. The

decrease in this case is due to heat conduction arising from the mild temperature gradient and negligible motion of the fluid with respect to the tank. When the direction of rotation of the spacecraft was reversed, however, a swirling motion of the fluid ensued as shown in figure 1.

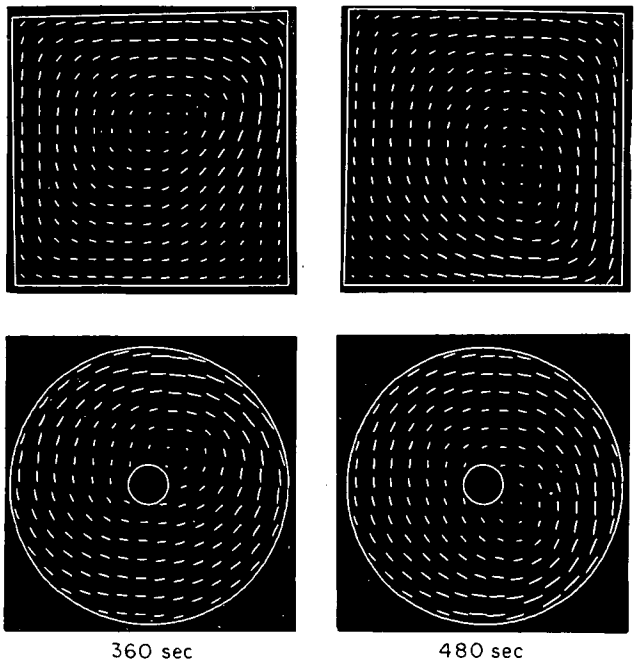

Figure 1. Velocity vectors for square and circular tanks showing clockwise swirl introduced by rotation reversal.

Photographs are presented of a cathode-ray display tube on which the velocity vectors are plotted at a number of points in the field. In the square tank, the velocity vectors are shown at the computational grid points. In the circular tank, the vectors are plotted at points in a rectangular array that does not correspond to computational grid points. This was done to avoid nonlinear concentrations of vectors in the display that would be difficult to view. Linear interpolation was used to obtain the values at the display points.

The upper and lower photographs on the left in figure 1 correspond to a time 360 sec after the rotation reversal. The photographs on the right show the velocity vectors 480 sec after reversal. The off-center swirls visible in these frames move continuously in a clockwise direction around the center in the same direction as the general motion of the fluid. The flow patterns in the square and circular tanks are similar as can also be seen in figures 2 and 3. The flow velocities are of order 0.003 m/sec (~0.01 ft/sec) near the outer boundaries.

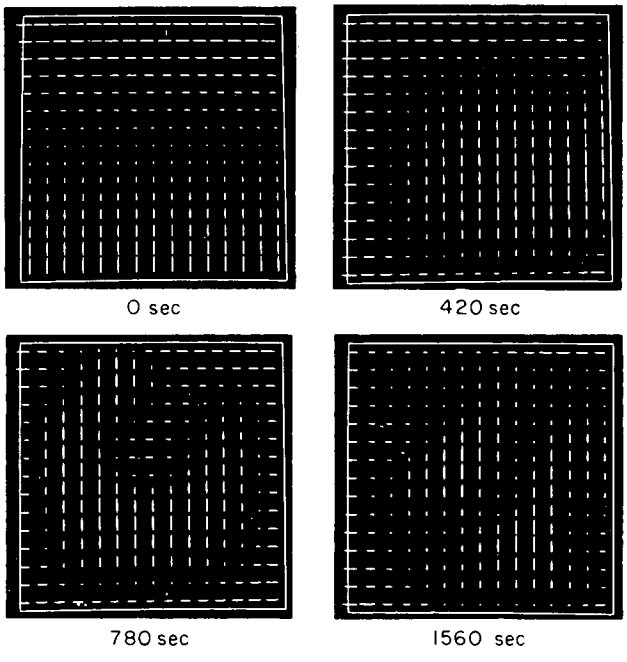

Figure 2. Temperature distributions after rotation reversal (square tank).

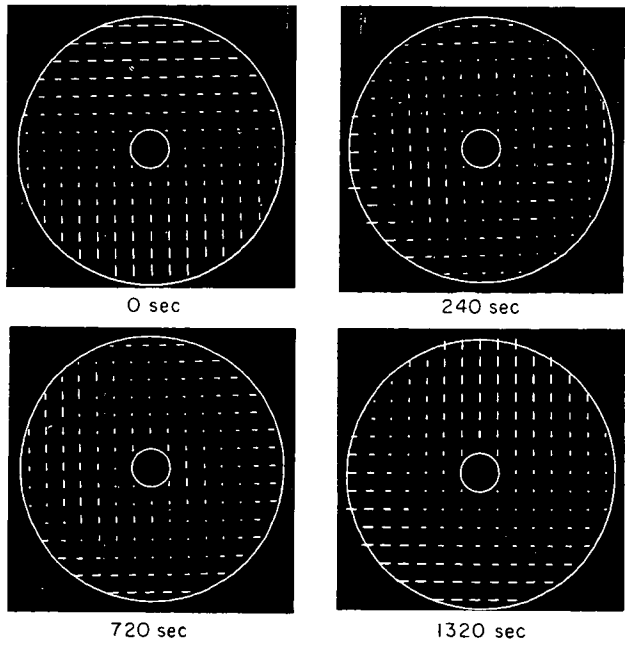

Figure 3. Temperature distributions after rotation reversal (circular tank).

Figure 2 shows a series of temperature distributions in a square tank. For temperatures greater than the average, the deviations from the mean are represented by vertical lines. As an aid to visualization, for temperatures less than average the deviations from the mean are shown as horizontal lines. In either case, the length of the line indicates the magnitude of deviation from the mean. The upper left photograph in figure 2 shows the initial assumed temperature distribution, which varies linearly from top to bottom. The warmer fluid (vertical lines) is toward the center of rotation, which is about 1-1/2 tank widths (diameters) below the center of the tank. The remaining photographs in figure 2 show the temperature distribution at later times after the rotation reversal. In the lower right photograph considerable mixing and dissipation of the temperature distribution have taken place. Figure 3 shows a similar evolution of temperature distributions in a circular tank resulting from a rotation reversal maneuver.

Figure 4 shows a comparison of the decreases in potential pressure decay (defined on p. 13) resulting from rotation reversal of square and circular tanks. These calculations were based on the van der Waals approximation of the thermodynamic properties of oxygen described in reference 12. No large difference in the degree of agreement exhibited for the two geometries is to be expected with the use of more accurate thermodynamic relations. No heater operation or heat leak were allowed for in these calculations and the pressure dropped to about 4.8×10^6 N/m^2 (~700 psi) near the ends of the runs. For such adiabatic mixing the decrease in potential pressure decay is equal to the drop in actual pressure. The initial linear temperature distribution for the circle was chosen to cover a larger range than that for the square so that the initial potential pressure decays would be equal. These results show that no large differences in the response of the fluid state to rotation reversal maneuvers are to be expected for square or circular geometry.

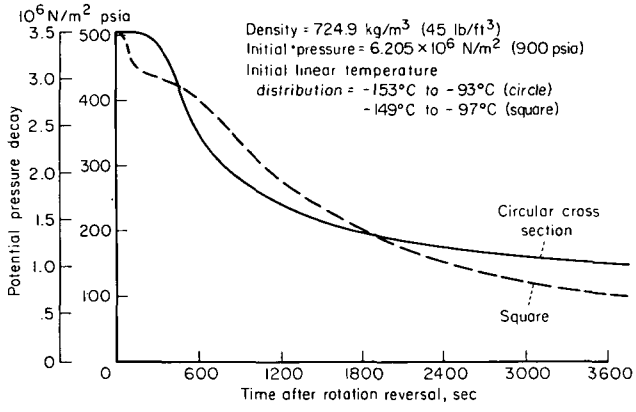

Figure 4. Comparison of reductions of potential pressure decay resulting from rotation reversal in square and circular tanks.

Heater Cycles

As discussed in references 10 and 12 and elsewhere, the Apollo oxygen tanks are equipped with heaters to overcome the drop in pressure from removal of fluid. Pressure sensors in the tanks turn the heaters on when the pressure falls below about 6.0×10^6 N/m^2 (~870 psia) and turn them off when the pressure rises above about 6.3×10^6 N/m^2 (~910 psia). During fluid removal, the heaters are thus automatically cyclically turned on and off about every 1200 sec, depending on the flow rate and the amount of fluid remaining. Figure 5 shows typical velocity and temperature fields that develop after several heater cycles for different simulated tank geometries and heater positions. The flow field in the upper left photograph was generated with elements on the left wall acting as a heater. A steady spacecraft rotation rate of 1.1111×10^{-4} revolutions per sec (0.4 rph) was imposed in all of the cases shown in figure 5. In the upper right photograph the velocity vectors resulting from an internal position of the heater are shown. In the lower left photograph, the velocity vectors generated in a circular tank with an internal heater position are shown for comparison. The lower

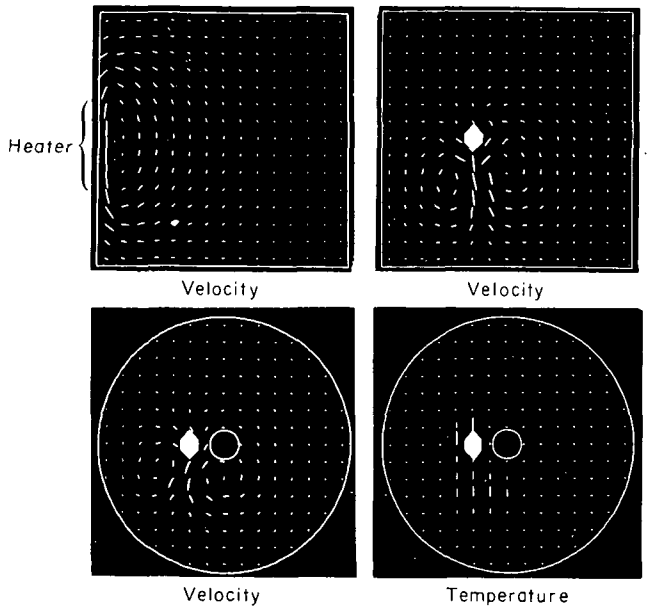

Figure 5. Velocity and temperature distributions resulting from heater operation with uniform rotation of the spacecraft at 1.1111×10^{-4} rps (0.4 rph) (hexagon denotes position of internal heater).

right frame shows the temperature distribution in the tank corresponding to the same calculation. In times of order 7200 sec (2 hr) with small spacecraft rotation rates, only a small volume of fluid near the heater is heated appreciably. It can be seen in the lower right photograph of figure 5 that the heated fluid tends to move toward the center of rotation, which is about 1-1/2 tank diameters below the center of the tank.

Figures 6, 7, and 8 show the pressure cycles and potential pressure decay versus time corresponding to the geometries of the upper left, upper right, and lower photographs in figure 5. In these calculations the accurate thermodynamic relations of Stewart (ref. 15) were used as described in references 11 and 12. In figure 6, the pressure rises when the heater is on and subsides when the heater is turned off. The lower plot of figure 6 shows that the potential pressure decay responds similarly, but also undergoes a cumulative rise as the amount of stratification increases. Comparison of figures 6, 7, and 8

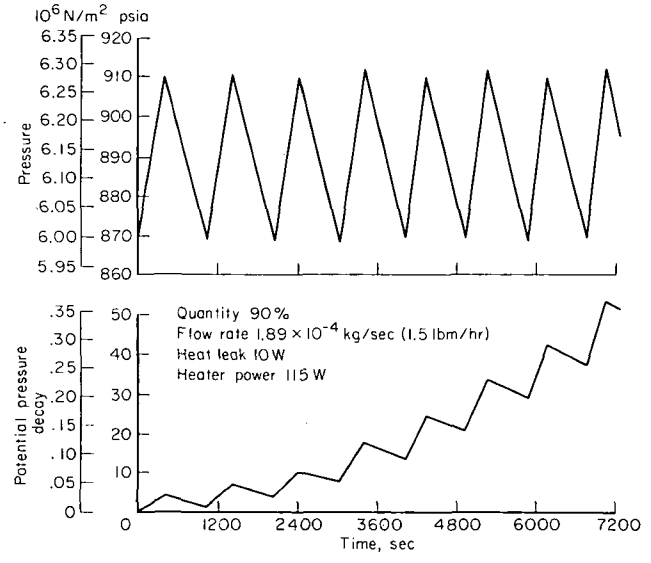

Figure 6. Pressure cycles for square tank with wall heater, rotation rate 1.1111×10^{-4} rps (0.4 rph).

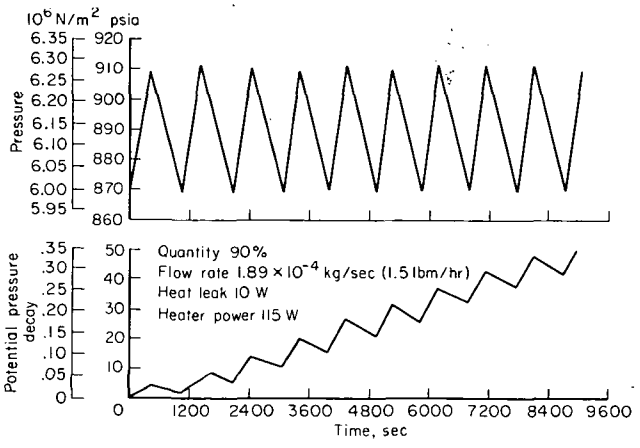

Figure 7. Pressure cycles for square tank with internal heater, rotation rate 1.1111×10^{-4} rps (0.4 rph).

shows that the response of pressure and potential pressure decay to heater cycling is insensitive to the geometry and position of the heater in the tank. The notation "Quantity 90%" in the figures indicates that the tanks contained 90 percent of the initial mass in these calculations. "Heat Leak 10 W" refers to the rate of heat leakage into the tank through the walls.

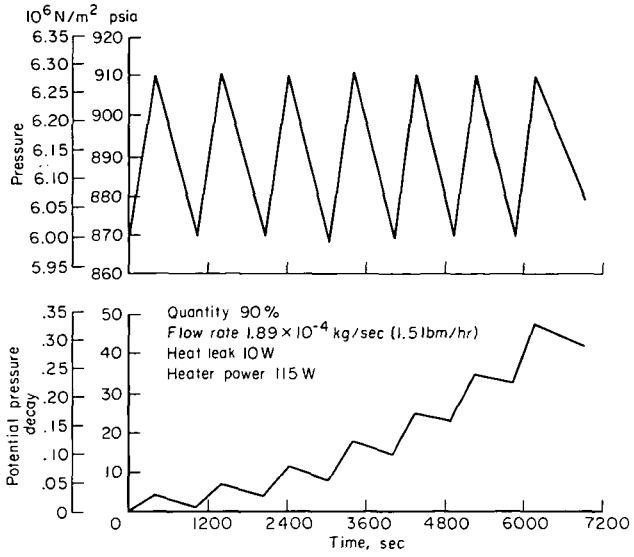

Figure 8. Pressure cycles for circular tank, rotation rate 1.1111×10^{-4} rps (0.4 rph).

Spin-Up Maneuver

Figure 9 shows the effect of vehicle spin-up on the pressure and potential pressure decay. In this calculation the spacecraft was not rotating initially and the cumulative rise of potential pressure decay was greater than in the previous figures, where the rate of rotation was 1.1111×10^{-4} rev/sec (0.4 rph). The spin-up was started at 7620 sec after the start of the calculation and was completed in about 300 sec. The rotation rate was held constant at 8.333×10^{-4} rev/sec (3 rph) thereafter. After a delay of 600 sec the swirling motion of the fluid introduced by the vehicle spin-up had a large effect on the pressure cycle. The delay can be attributed to the fact that the initial response of the fluid was essentially a solid body rotation relative to the tank. A period of time elapsed before the interaction of density gradients with the new acceleration field resulted in nonuniform motion of the fluid. The resulting mixing action caused a drop in pressure and also reduced the potential pressure decay. Thus, even though the heater was turned on at 8940 sec, when the pressure fell below 6.00×10^6 N/m^2 (870 psia), it continued to drop because of the mixing action and was down to 5.58×10^6 N/m^2 (810 psia) at the end of the calculation. The calculation ended at that time because of failure to allow for lower pressures in the machine code as described in reference 12. A similar drop in potential pressure decay and pressure resulting from spin-up after heater cycling was obtained for a square tank in reference 10, showing that the effect is insensitive to the geometry (square or circular) used in the calculation. These results also show that the potential pressure decay associated with local hot spots produced by heater cycling is more effectively removed by spacecraft maneuvering than a linear temperature distribution across the entire tank.

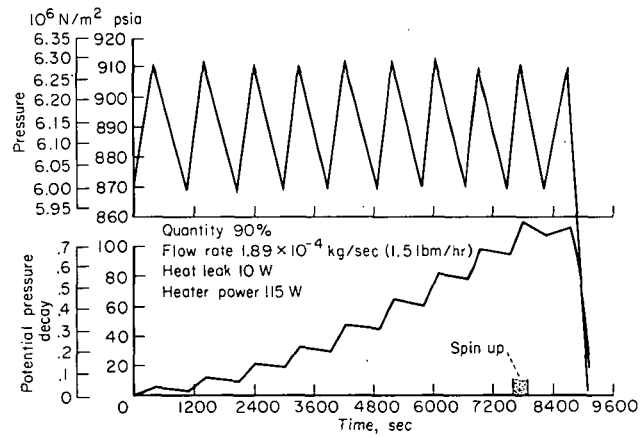

Figure 9. Effect of spin-up on pressure cycle (circular tank, initial rotation rate 0, final rotation rate 8.333×10^{-4} rps or 3 rph).

This can be seen by comparison of figures 4 and 9. In figure 9 the onset of an appreciable decrease in potential pressure decay occurs more quickly and the decrease is more rapid.

DISCUSSION

The foregoing results show that appreciable mixing can be achieved in a short time by changing the spacecraft rotation rate by modest amounts. No significant differences were found in the calculations for circular geometry in this report and those for a square tank in reference 10. As discussed in reference 10, to obtain numerical stability in the flow near the corners of a square tank it was found expedient to put an upper limit on vorticity. The upper limit imposed was four times the value corresponding to the solid body rotation of the fluid associated with a rotation reversal from 8.333×10^{-4} rev/sec (3 rph) to 3 rph in the opposite direction. This limit on the absolute value of vorticity also resulted in slip flow in the boundary layer near the walls. It was argued that the resulting obscuration of possible reversed flow eddies in the corners is not objectionable since the actual tanks being simulated are spherical and do not have corners. It was also demonstrated by estimates based on flow over a flat plate that the boundary layer at the walls would remain relatively thin during times simulated by the computations. Therefore, the slip flow at the walls resulting from the imposition of an upper limit on vorticity would affect the motion of only a small fraction of the total volume of fluid. It was concluded that the calculations for a square tank provide conservative estimates of the mixing induced in the main bulk of fluid by the interaction of density gradients with the acceleration field due to spacecraft maneuvering. Nevertheless, it was deemed worthwhile to make calculations for a circular tank to determine whether the methods used to suppress corner flow effects could cause errors that had not been recognized. (In the circular-tank calculations, the limiting values of vorticity did not occur except right on the boundaries.)

The present calculations for circular tanks in which no large differences were found relative to the earlier calculations for square tanks reinforces the conclusions derived from the square-tank calculations. The levels of potential pressure decay to be anticipated according to our calculations are in reasonable agreement with previous estimates from Apollo 12 data and stratification analyses (see ref. 10). We concur in the conclusion that dangerous levels of stratification will not occur with mass flow rates and acceleration fields corresponding to past and anticipated Apollo operational practices.

Ames Research Center
National Aeronautics and Space Administration
Moffett Field, Calif. 94035, June 28, 1972

REFERENCES

1. Computational Fluid Dynamics Branch of Ames Research Center: Convection in the Tanks of a Rotating Spacecraft. NASA TR R-386, 1972.

2. Martin, E.D.: An Overview of the Rotating Spacecraft Tank Convection Problem. NASA TR R-386, 1972, Ch. 1 pp. 1–7.

3. Kamat, D. V.; and Abraham, W. H.: Pressure Collapse in Oxygen Storage under Zero-g. J. Spacecraft, 5, 184, 1968.

4. Martin, E. D.; and Baldwin, B. S.: Flow Equations Governing Combined Forced and Natural Convection for Application in a Rotating Tank. NASA TR R-386, 1972, Ch. 2 pp. 9–37.

5. Ostrach, Simon: Laminar Flows With Body Forces. Section F in Theory of Laminar Flows, F. K. Moore, ed., Vol. IV of High Speed Aerodynamics and Jet Propulsion, Princeton Univ. Press, 1964, pp. 528–718.

6. Greenspan, H. P.: The Theory of Rotating Fluids. Cambridge Univ. Press, 1968.

7. Briley, W. R.; and Walls, H. A.: A Numerical Study of Time-Dependent Rotating Flow in a Cylindrical Container at Low and Moderate Reynolds Numbers. Proc. Second Int. Conf. on Numerical Methods in Fluid Dynamics, Sept. 15–19, 1970, Univ. of Calif., Berkeley, M. Holt, ed. (Lecture Notes in Physics, vol. 8) Springer-Verlag, Berlin, 1971.

8. Lighthill M. J.: Introduction. Boundary Layer Theory. Section II in Laminar Boundary Layers, L. Rosenhead, ed., Oxford, Clarendon Press, 1963, pp. 46–113.

9. Lomax, H.; and Bailey, F. R.: Computational Method for Calculating Convection in a Rotating Tank. NASA TR R-386, 1972, Ch. 3 pp. 39–59.

10. Baldwin, B. S.; Reinhardt, W. A.; and Sheaffer, Y. S.: Results from Numerical Computations Simulating Flows in an Apollo Oxygen Tank. NASA TR R-386, 1972, Ch. 6 pp. 123–127.

11. Reinhardt, W. A.: Calculation of Thermodynamic Properties of Oxygen Near the Critical Point. NASA TR R-386, 1972, Ch. 4 pp. 61–97.

12. Baldwin, B. S.; Reinhardt, W. A.; and Sheaffer, Y. S.: Analysis of Thermodynamic States Resulting from Small-Density-Variation Approximation of Fluid Motion in Cryogenic Oxygen Tanks. NASA TR R-386, 1972, Ch. 5, pp. 99–121.

13. MacCormack, R. W.: The Effect of Viscosity in Hypervelocity Impact Cratering. AIAA paper 69–354, 1969.

14. Hockney, R. W.: The Potential Calculation and Some Applications, In *Methods in Computational Physics*, vol. 9 (B. Alder, S. Fernbach, and M. Rotenberg, eds.), Academic Press, N.Y., pp. 135–211, 1970.

15. Stewart, R. B.: The Thermodynamic Properties of Oxygen. Ph.D. Thesis, Dept. of Mech. Eng., Univ. Iowa, 1966.

NATIONAL AERONAUTICS AND SPACE ADMINISTRATION
WASHINGTON, D.C. 20546

OFFICIAL BUSINESS
PENALTY FOR PRIVATE USE $300

SPECIAL FOURTH-CLASS RATE
BOOK

POSTAGE AND FEES PAID
NATIONAL AERONAUTICS AND
SPACE ADMINISTRATION
451

U.S.MAIL

POSTMASTER: If Undeliverable (Section 158 Postal Manual) Do Not Return

"The aeronautical and space activities of the United States shall be conducted so as to contribute . . . to the expansion of human knowledge of phenomena in the atmosphere and space. The Administration shall provide for the widest practicable and appropriate dissemination of information concerning its activities and the results thereof."

—NATIONAL AERONAUTICS AND SPACE ACT OF 1958

NASA SCIENTIFIC AND TECHNICAL PUBLICATIONS

TECHNICAL REPORTS: Scientific and technical information considered important, complete, and a lasting contribution to existing knowledge.

TECHNICAL NOTES: Information less broad in scope but nevertheless of importance as a contribution to existing knowledge.

TECHNICAL MEMORANDUMS: Information receiving limited distribution because of preliminary data, security classification, or other reasons. Also includes conference proceedings with either limited or unlimited distribution.

CONTRACTOR REPORTS: Scientific and technical information generated under a NASA contract or grant and considered an important contribution to existing knowledge.

TECHNICAL TRANSLATIONS: Information published in a foreign language considered to merit NASA distribution in English.

SPECIAL PUBLICATIONS: Information derived from or of value to NASA activities. Publications include final reports of major projects, monographs, data compilations, handbooks, sourcebooks, and special bibliographies.

TECHNOLOGY UTILIZATION PUBLICATIONS: Information on technology used by NASA that may be of particular interest in commercial and other non-aerospace applications. Publications include Tech Briefs, Technology Utilization Reports and Technology Surveys.

Details on the availability of these publications may be obtained from:

SCIENTIFIC AND TECHNICAL INFORMATION OFFICE

NATIONAL AERONAUTICS AND SPACE ADMINISTRATION

Washington, D.C. 20546